Ribose 2′-O-methylation provides a molecular signature for the distinction of self and non-self mRNA dependent on the RNA sensor Mda5

Article

Accepted Version

Ribose 2'-*O*-methylation provides a molecular signature for MDA5-dependent distinction of self and non-self mRNA

Roland Züst[1#], Luisa Cervantes-Barragan[1#], Matthias Habjan[1], Reinhard Maier[1], Benjamin W. Neuman[2], John Ziebuhr[3,4], Kristy J. Szretter[5], Susan C. Baker[6], Winfried Barchet[7], Michael S. Diamond[5], Stuart G. Siddell[8], Burkhard Ludewig[1,9] and Volker Thiel[1,9*]

[1]Institute of Immunobiology, Kantonal Hospital St. Gallen, St. Gallen, Switzerland. [2]School of Biological Sciences, University of Reading, United Kingdom. [3]Centre for Infection and Immunity, Queen's University Belfast, Belfast United Kingdom. [4]Institute of Medical Virology, Justus Liebig University Giessen, Giessen, Germany. [5]Departments of Medicine, Molecular Microbiology, and Pathology & Immunology, Washington University School of Medicine, St Louis, MO 63110, USA. [6]Department of Microbiology and Immunology, Loyola University Stritch School of Medicine, Maywood, Illinois, USA. [7]Institute for Clinical Chemistry and Pharmacology, University Hospital, University of Bonn, Germany [8]Department of Cellular and Molecular Medicine, School of Medical and Veterinary Sciences, University of Bristol, Bristol, United Kingdom. [9]Vetsuisse Faculty, University of Zürich, Switzerland.

Running Title: Evasion of innate immune sensing by viral RNA 2'-*O*-methylation

Key words: Interferon, MDA5, coronavirus, RNA methylation, 2'-*O*-methyltransferase

[*]**Corresponding author:**

Volker Thiel; Kantonal Hospital St.Gallen, Institute of Immunobiology, 9007 St.Gallen, Switzerland. Phone: +41-71-4942843; fax: +41-71-4946321; e-mail: volker.thiel@kssg.ch

# R.Z. and L.C-B contributed equally to this work.

ABSTRACT

The 5'-cap-structures of higher eukaryote mRNAs are ribose 2'-*O*-methylated. Likewise, a number of viruses replicating in the cytoplasm of eukayotes have evolved 2'-*O*-methyltransferases to modify autonomously their mRNAs. However, a defined biological role of mRNA 2'-*O*-methylation remains elusive. Here we show that viral mRNA 2'-*O*-methylation is critically involved in subversion of type-I-interferon (IFN-I) induction. We demonstrate that human and murine coronavirus 2'-*O*-methyltransferase mutants induce increased IFN-I expression, and are highly IFN-I sensitive. Importantly, IFN-I induction by 2'-*O*-methyltransferase-deficient viruses is dependent on the cytoplasmic RNA sensor melanoma differentiation-associated gene 5 (MDA5). This link between MDA5-mediated sensing of viral RNA and mRNA 2'-*O*-methylation suggests that RNA modifications, such as 2'-*O*-methylation, provide a molecular signature for the discrimination of self and non-self mRNA.

INTRODUCTION

Innate immune recognition of pathogen-associated molecular patterns (PAMPs) facilitates the distinction between immunological self and non-self[1]. In the case of cytoplasmic viral RNA, this involves detection by cytoplasmic RIG-I-like receptors (RLRs), such as retinoic acid-inducible gene-I (RIG-I) and MDA5. RLR activation results in the initiation of signaling cascades that induce the expression of cytokines, including IFN-I. These interferons, mainly IFN-α and IFN-β, are secreted and can then bind to the IFN-I receptor (IFNAR) and thus transmit a danger signal to neighboring cells. The activated IFNAR triggers the JAK-STAT signaling pathway, inducing the expression of a large array of IFN-stimulated genes (ISGs) with antiviral activity, thus establishing the so-called host cell antiviral state[2-4]. These ISGs include the protein kinase PKR, and stress-inducible proteins, such as interferon-induced protein with tetratricopeptide repeats (IFIT) 1 and IFIT2 (also known as ISG56 and ISG54, respectively), which impair the host cell protein synthesis apparatus[4-7].

Although the distinction between self and non-self RNA is believed to rely on the molecular signatures found in PAMPs, the exact nature of such signatures remains elusive. Both of the cytosolic RLRs, RIG-I and MDA5, have been shown to bind to double-stranded (ds) RNA with the difference that RIG-I appears to prefer short dsRNA, whereas MDA5 can specifically bind long dsRNA[8]. In addition, the 5'-end of RNAs is currently receiving increased attention, as it has been shown that RIG-I can specifically recognize 5'-triphosphate groups on single-stranded and (partially) dsRNAs[9-11]. In contrast, eukaryotic mRNAs, which are not recognized by RIG-I or MDA5, usually have a 5'-cap structure that is methylated at the N-7 position of the capping guanosine residue (cap 0), the ribose-2'-*O* position of the 5'-penultimate residue (cap 1) and sometimes at adjoining residues (cap 2)[12]. There are two evolutionary forces proposed to be responsible for the presence of 5'-cap structures on eukaryotic mRNAs, namely the appearance of 5'-exonucleases in eukaryotes, and as means of directing mRNA to the eukaryotic ribosome[13].

Thus, eukaryotic mRNA 5'-cap structures are known to increase mRNA stability and translational efficacy. Notably, although N7-methylation has been implicated to be important in many mRNA-related processes, such as transcriptional elongation, polyadenylation, splicing, nuclear export, and efficient translation, there is no obvious indication why higher eukaryotes have evolved mRNA ribose-2'-*O*-methylation in cap 1 and cap 2 structures.

The functional significance of mRNA 5'-structures is best illustrated by the fact that many viruses that replicate in the cytoplasm have evolved either alternative 5'-elements, such as small viral proteins linked to the 5'-end of genomic RNA[14], or encode functions associated with 5'-cap formation that are homologous to those found in eukaryotic cells, such as RNA 5'-triphosphatase, RNA guanylyltransferase, RNA guanine-N7-methyltransferase (N7-MTase), and 2'-*O*-MTase (e.g. flaviviruses, coronaviruses and poxviruses) (**Fig 1, Supplementary Table 1**). In addition to the well-established role of mRNA 5'-structures in translation, the discovery that RNA 5'-triphosphate groups activate RIG-I[9,10] suggests that viruses have to hide or modify their RNA 5'-structures to evade innate immune recognition. Interestingly, RIG-I activation is diminished when 5'-triphosphate RNA contains modified nucleotides[9]. Thus, we hypothesize that RNA modifications, such as methylation, could be a critical factor for the activation of RNA-specific pattern recognition receptors (PRRs). Notably, this concept of methylation-based distinction of self and non-self nucleic acids is well-established for DNA, since the methylation status of CpG motifs in DNA is the structural basis of toll-like receptor (TLR) 9 activation[15]. Moreover, DNA methylation has long been recognized as the basis for the ancient bacterial restriction and modification systems that allow bacteria to distinguish between foreign DNA and the bacterial genome.

Here, we show that viral mRNA 2'-*O*-methylation is biologically significant in the context of host cell innate immune responses. We demonstrate that human and murine coronavirus mutants lacking 2'-*O*-MTase activity induce increased IFN-I expression and are extremely

sensitive to IFN-I treatment. Furthermore, we show that a murine coronavirus mutant with an inactivated 2'-*O*-MTase is attenuated in wild type (WT) macrophages but replicates efficiently in the absence of IFN-I receptor or MDA5. Consonantly, coronavirus 2'-*O*-MTase mutants are apathogenic in WT mice but virus replication and spread is restored in mice lacking the IFN-I receptor and in mice lacking the two major sensors of coronaviral RNA, TLR7 and MDA5. Collectively, our results reveal a link between MDA5-mediated sensing of viral RNA and mRNA 2'-O-methylation, and suggest that RNA modifications, such as 2'-O-methylation, provide a molecular signature for the distinction of self and non-self mRNA.

RESULTS

Effects of 2'-*O*-MTase-deficiency in human coronavirus infection

To address the biological significance of mRNA 2'-*O*-methylation in the context of host cell innate immune responses, we first used a human model of coronavirus infection. Coronaviruses are single-strand (+) RNA viruses, that replicate in the cytoplasm, and have evolved N-7 and 2'-*O*-MTases to methylate their viral mRNA 5'-cap structures[16-19]. The 2'-*O*-MTase activity is associated with the viral non-structural protein (nsp) 16, which is highly conserved amongst coronaviruses (**Fig. 1a,b**) and an integral subunit of the viral replicase-transcriptase complexes located at virus-induced double membrane vesicles (DMVs) in the host cell cytoplasm. We have generated a recombinant *human coronavirus* strain 229E (HCoV-229E) mutant encoding an inactivated 2'-*O*-MTase. This mutant, HCoV-D129A, was produced by substituting nsp16 residue D129 of the highly conserved catalytic K-D-K-E tetrad with alanine (**Fig 1b**). Importantly, this substitution has been shown to completely abrogate 2'-*O*-MTase activity of recombinant, bacterial-expressed feline coronavirus and SARS coronavirus nsp16 proteins[16,18]. The mutant virus displayed a small plaque phenotype, and reduced replication in the human fibroblast MRC-5 cell line (**Fig 2a,b**). Moreover, we could readily 2'-*O*-methylate poly(A)-containing RNA obtained from HCoV-D129A-infected cells using the vaccinia virus 2'-*O*-MTase VP39[20] *in vitro* (**Fig 2c**), confirming the loss of 2'-*O*-MTase activity. In contrast, *in vitro* 2'-*O*-methylation of poly(A)-containing RNA derived from HCoV-229E-infected cells was indistinguishable compared to poly(A)-containing RNA obtained from mock infected cells. Importantly, compared to HCoV-229E, we observed significantly increased IFN-β expression in blood-derived human macrophages (MΦs) following HCoV-D129A infection (**Fig 2d**), and complete restriction of HCoV-D129A replication in human MΦ that had been pretreated with IFN-α (**Fig 2e**). These results suggest a biological role of mRNA 2'-*O*-methylation in the context of (i) IFN-I induction, and (ii) IFN-I stimulated antiviral effector mechanisms.

127

128 **IFN-I induction by 2'-*O*-MTase mutants is MDA5-dependent**

129 To extend our studies on the impact of 2'-*O*-methylation on coronavirus-induced innate
130 immune responses, we used an animal model of coronavirus infection with *mouse hepatitis virus*
131 strain A59 (MHV-A59) as a natural mouse pathogen. Studies on innate immune responses
132 following MHV-A59 infection have shown that plasmacytoid dendritic cells (pDCs) have a
133 unique and crucial role in sensing coronaviral RNA via TLR7, ensuring a swift production of
134 IFN-I following virus encounter[21,22]. Other target cells, such as primary fibroblasts, neurons,
135 astrocytes, hepatocytes, and conventional dendritic cells, do not produce detectable IFN-I upon
136 MHV infection[22,23]. The exceptions are MΦs and microglia, which can respond with IFN-I
137 expression upon MHV infection, although only to moderate levels[24,25]. Importantly however,
138 IFN-I expression detected in MΦs and microglia is dependent on MDA5[24].

139 We have generated a recombinant MHV lacking 2'-*O*-MTase activity by substituting the
140 nsp16 2'-*O*-MTase active site residue D130 with alanine (MHV-D130A; **Fig 1b**). In addition, we
141 generated a recombinant MHV mutant, designated MHV-Y15A, encoding a Y15A substitution
142 at the putative type 0 cap binding site of nsp16 (**Fig 1b**). This substitution was shown to impair
143 type 0 cap-binding for the corresponding feline coronavirus nsp16 mutant Y14A[18], and we
144 expected that this substitution would reduce, rather than completely abrogate coronaviral mRNA
145 2'-*O*-methylation. Indeed, the *in vitro* methylation of mRNA with the vaccinia virus 2'-*O*-MTase
146 VP39[20] confirmed the differential 2'-*O*-methylation of mRNA obtained from MHV-infected
147 cells. As shown in **Figure 3a**, right panel, transfer of [^{3}H]-labeled methyl groups from the
148 methyl donor S-adenosyl-methionine (SAM) to mRNA derived from MHV-Y15A-infected cells
149 was less efficient compared to MHV-D130A mRNA, but significantly increased compared to
150 MHV-A59 mRNA. These results show the loss of 2'-*O*-MTase activity of MHV-D130A, and
151 that a significant proportion of MHV-Y15A mRNA is not methylated at the 2'-*O* position.

The analysis of virus growth in cell culture revealed that the replication kinetics of both recombinant viruses, MHV-D130A and MHV-Y15A, differed only slightly from those of MHV-A59 following infection of a murine fibroblast 17Cl-1 cell line with high and low multiplicities of infection (MOI; MOI=1 and MOI=0.0001, respectively) (**Fig 3b**). Also, there was no significant difference observed in electron microscope analyses of DMV formation and morphology in the cytoplasm of MHV-A59-, MHV-D130A-, and MHVY15A-infected cells (**Supplementary Fig 1**), which is relevant in relation to cytoplasmic viral RNA sensing, since coronavirus DMVs are known to harbor dsRNA. When we analyzed IFN-I in supernatants of WT MΦs at 15 hours p.i., we observed that infection with both 2'-*O*-MTase mutants, MHV-Y15A and MHV-D130A, resulted in increased IFN-I production (**Fig 3c, Supplementary Fig 2a**). Likewise, IFN-I was efficiently produced in MHV-D130A and MHV-Y15A infected IFNAR-deficient MΦs compared to MHV-A59 infection, demonstrating that increased IFN-I production by MHV 2'-*O*-MTase mutants is detectable in the absence of IFNAR signaling (**Fig 3d, Supplementary Figure 2b**). Importantly, in MDA5-deficient MΦs neither MHV-A59, nor the two 2'-*O*-MTase mutant viruses induced any detectable expression of IFN-I (**Fig 3e**), whereas IFN-I production was readily detectable in MDA5-deficient cells following Sendai virus infection. Detailed analysis of IFN-β mRNA expression kinetics revealed that infection of WT (**Fig 3f**) and IFNAR-deficient (**Fig 3g**) MΦs with both MHV-D130A and MHV-Y15A resulted in increased IFN-β gene expression with a peak at 12 h p.i.. Notably, IFN-β induction was most pronounced after infection with the 2'-*O*-MTase active site mutant MHV-D130A. These results indicate that the level of IFN-β expression correlates with the degree of 2'-*O*-methylation deficiency of viral RNA and, that IFN-β induction following infection with 2'-*O*-MTase mutant viruses is MDA5-dependent. Consonantly, we observed increased nuclear localization of interferon regulatory factor 3 (IRF3; a transcription factor that is activated in the RLR signaling

pathway and is translocated from the host cell cytoplasm to the nucleus to mediate IFN-I transcription) in MHV-D130A- and MHV-Y15A-infected IFNAR-deficient MΦs, but not in MDA5-deficient MΦs (**Fig 4**). Collectively, these results demonstrate a linkage of mRNA 2'-*O*-methylation and MDA5-dependent induction of IFN-β expression.

2'-*O*-methylation affects two distinct antiviral mechanisms

Since the 2'-*O*-MTase active site mutant HCoV-D129A displayed an elevated sensitivity to IFN-I treatment, we assessed whether IFN-I induced restriction of viral replication is also effective against the MHV 2'-*O*-MTase mutants. Therefore, we investigated in more detail the viral replication kinetics of MHV-D130A and MHV-Y15A in primary MΦs, which represent the most important target cells for MHV [21,26]. MHV-D130A replication was greatly impaired in WT MΦs (even after infection with high MOI; MOI=1), whereas replication of MHV-Y15A was similar to that of MHV-A59 (**Fig 5a**). Importantly, MHV-D130A replication was fully restored in MDA5-deficient MΦs, even after infection with low MOI (MOI=0.0001) (**Fig 5b**). This demonstrates that MDA5-dependent IFN-I expression is a prerequisite for the induction of effective restriction of MHV-D130A replication. In agreement with the notion that the replication of MHV-D130A, but not MHV-Y15A, was impaired in WT MΦs, we observed a remarkable reduction of MHV-D130A replication in WT MΦs that were pretreated with IFN-α. Thus, compared to MHV-A59, MHV-D130A replication was not detectable at 24 h p.i. (after 4 h pretreatment of WT MΦs with 50 - 200 U IFN-α), whereas MHV-Y15A replication was not significantly restricted (**Fig 5c**). Interestingly, in MDA5-deficient MΦs, pretreatment with at least 200 U IFN-α was required to restrict MHV-D130A replication to non-detectable levels (**Fig 5d**). This suggests that endogenous MDA5-mediated IFN-I expression additionally impacts on MHV-D130A restriction in WT MΦs. Collectively these analyses depict a clear difference

between the phenotypes of MHV-D130A and MHV-Y15A. Inactivation of the MHV 2'-*O*-MTase activity by targeting the active site residue D130 led to increased IFN-I production as well as to pronounced sensitivity to IFN-I pretreatment. In contrast, reduction of viral mRNA 2'-*O*-methylation through targeting of the type 0 cap-binding site residue Y15 was sufficient to induce increased IFN-I production but not to confer increased IFN-I sensitivity. Thus, we conclude that there is, in addition to MDA5-dependent IFN-I induction, a second and distinct antiviral mechanism, which is IFN-I-induced and accounts for the restriction of viral replication during the host cell antiviral state.

In this respect, Daffis and colleagues have shown recently that the replication of a West Nile virus (family *Flaviviridae*, genus flavivirus) mutant lacking 2'-*O*-methylation was strongly inhibited by IFIT gene family members[27], which are ISGs implicated in translational regulation. To assess whether this molecular mechanism also pertains to coronavirus infection, we assessed the replication kinetics of MHV-A59, MHV-D130A, and MHV-Y15A in primary MΦs derived from WT or *ifit1*$^{-/-}$ mice. Remarkably, MHV-D130A replication was almost completely restored in *ifit1*$^{-/-}$ MΦs (**Fig 6**), analogous to the restoration of MHV-D130A replication in *mda5*$^{-/-}$ MΦs (**Fig 5a,b**). Collectively, these findings show that the MDA5-dependent IFN-I induction and the IFIT-1-mediated restriction of viral replication are two distinct antiviral mechanisms that are both based on the distinction of 2'-*O*-methylated and non-methylated mRNAs, but operate at different levels of the host cell antiviral response.

Impact of 2'-*O*-MTase-deficiency on innate immune recognition *in vivo*

Next, we examined the impact of viral mRNA 2'-*O*-methylation on innate immune recognition and virulence *in vivo* and compared the phenotype of MHV-A59 with those of the MHV 2'-*O*-MTase mutants in C57BL/6 (B6) mice after intraperitoneal (i.p.) infection with 500 plaque forming units (p.f.u.) of virus (**Fig 7a,b**). In contrast to MHV-A59, neither of the MHV

225 2'-*O*-MTase mutants were detectable in spleens or livers of B6 mice at 48 h.p.i., demonstrating
226 the importance of viral mRNA 2'-*O*-methylation for efficient replication and spread in the host.
227 Moreover, both MHV 2'-*O*-MTase mutants could replicate and spread in IFNAR-deficient mice,
228 emphasizing the pivotal role of viral mRNA 2'-*O*-methylation as a countermeasure to the host
229 IFN-I response. Finally, in MDA5-deficient and TLR7-deficient mice, the two known receptors
230 recognizing coronaviral RNA, and consonant with the pronounced sensitivity of the 2'-*O*-MTase
231 active site mutant MHV-D130A to IFN-α pretreatment in MΦs, MHV-D130A was not
232 detectable in spleens or livers of mice lacking either of the RNA sensors. This suggested that
233 induction of IFN-I expression via TLR7 or MDA5 suffices to completely restrict viral replication
234 and spread when viral mRNA 2'-*O*-methylation is abrogated. Interestingly, the type 0 cap-
235 binding mutant MHV-Y15A was still detectable in the spleens of TLR7-deficient and MDA5-
236 deficient mice, suggesting that robust IFN-I induction by both RNA sensors is required to fully
237 restrict viral replication if the 2'-*O*-MTase activity is reduced rather than abrogated. Importantly,
238 in mice deficient for both receptors, TLR7 and MDA5 ($tlr7^{-/-}/mda5^{-/-}$), the replication and spread
239 of both MHV 2'-*O*-MTase mutants was indistinguishable compared to IFNAR-deficient mice.
240 These observations confirm that TLR7 and MDA5 represent the main sensor molecules for
241 recognizing coronaviral RNAs and demonstrate that 2'-*O*-methylation of viral mRNA serves as a
242 mechanism to evade host innate immune recognition of non-self RNA *in vivo*.
243
244

DISCUSSION

The correct functioning of host innate immune responses is based on reliable pathogen detection and is essential in limiting pathogen replication and spread. Here, we demonstrate by using human and murine coronavirus models of infection that mRNA 2'-*O*-methylation provides a molecular signature that has a dual role during interaction with the host innate immune responses. First, mRNA 2'-*O*-methylation protects viral RNA from recognition by MDA5 and thus prevents MDA5-dependent IFN-I production in virus-infected cells. Second, 2'-*O*-methylation of viral mRNA contributes to evasion from the IFIT1-dependent restriction of viral replication that is operative during the IFN-I-induced host cell antiviral state. Moreover, this study shows that these distinct processes can be uncoupled either in the absence of IFN-I signaling (e.g. in IFNAR-deficient cells/mice), or through a genetic approach that targets the cap-0 binding residue Y15 of MHV nsp16. Apparently, the lack of 2'-*O*-methylation on a proportion of MHV-Y15A mRNAs is sufficient to trigger the MDA5 pathway of IFN-I induction, whilst the MHV-Y15A mRNAs that are 2'-*O*-methylated allows the virus to evade the IFIT-1-mediated restriction of viral replication. In contrast, the absence of 2'-*O*-methylation of viral RNA through targeting of the 2'-*O*-MTase active site residue D130 strongly activates the MDA5 pathway and results in restriction of virus propagation.

The data provided in this study elucidate the impact of mRNA 2'-*O*-methylation on MDA5-dependent induction of IFN-I. The use of human and murine systems of coronavirus infection greatly facilitated the analysis of this link because (i) coronaviruses encode their own 5' mRNA cap methylation machinery, which allowed us to study the phenotype of recombinant viruses with mutated 2'-*O*-MTase proteins, and (ii) the induction of IFN-I expression is hardly detectable in infected cells, other than pDCs, with the notable exception of MΦs, which produce a low level of MDA5-mediated IFN-I following infection[22-24,28]. In contrast, most other RNA viruses that replicate in the cytoplasm induce considerable levels of IFN-I that may mask the

specific impact of mRNA 2'-*O*-methylation on MDA5 activation[2,29]. In future studies it will be important to clarify whether viral mRNA lacking 2'-*O*-methylation is directly recognized by MDA5, resulting in its activation, or whether it is part of the activation signal of MDA5, possibly in combination with dsRNA regions. The reverse genetic approach used in this study provided evidence for the biological significance of mRNA 2'-*O*-methylation in the context of MDA5-dependent IFN-I induction, and we expect that the generation of further recombinant viruses, harboring defined mutations in RNA-processing enzymes, combined with biochemical approaches will be useful in the identification of naturally occurring MDA5 ligands.

The evasion of MDA5-dependent RNA recognition and IFIT gene member dependent restriction of virus replication provide a reasonable explanation for the conservation of 2'-*O*-MTases in many viruses replicating in the cytoplasm of higher eukaryotes (**Supplementary Table 1**). It is also striking that a number of viruses, such as bunyaviruses and arenaviruses, which replicate in the cytoplasm but have not acquired the ability to autonomously generate and modify their 5'-cap structures, have evolved means to snatch the cap structure from cellular mRNA[30,31] (**Supplementary Table 1**). Moreover, structural and functional analyses of the Lassa virus (family *Arenaviridae*) nucleoprotein have revealed that this cap-binding protein can antagonize IFN-I through its associated 3' – 5' exoribonuclease activity, probably by cleaving RNAs that function as PAMPs[32]. The protein also has an unusually deep cap-binding pocket that has been proposed to accommodate the entire m7GpppN cap structure[32]. Thus it is potentially able to recognize and discriminate between 2'-*O*-methylated and non-methylated capped RNAs. Finally, members of the *Picornavirales* order and related viruses, which replicate in the cytoplasm but do not encode MTases, have evolved alternative 5'-ends of their viral RNAs. These viruses covalently attach a small viral protein (VPg) to the genomic 5'-terminus and harbor an internal ribosomal entry site at the 5'-non-tranlated region[33] (**Supplementary Table 1**). Interestingly, encephalomyocarditis virus (EMCV, family *Picornaviridae*) replication appears

295 not to be restricted by IFIT proteins[27], however, EMCV infection is sensed through the MDA5
296 pathway[34]. Thus, it is tempting to speculate, that the use of internal ribosomal entry allows
297 EMCV to evade host restriction by IFIT family members, but the covalent attachment of VPg to
298 picornaviral RNA 5'-termini does not prevent MDA5-dependent RNA recognition and IFN-I
299 induction.

300 A relationship between RNA modification and host cell innate immune responses is further
301 supported by observations made during studies of cellular PRRs. For example, it has been shown
302 that activation of RIG-I and PKR is diminished when 5' triphosphate RNA contains modified
303 nucleotides[9,10,35]. Similarly, nucleoside modifications reduce the potential of RNA to trigger
304 TLRs[36]. Although, most of these observations have been made by in vitro studies (e.g. the
305 transfection of short synthetic RNAs), it appears that RNA modifications may impact on innate
306 immune sensing on a wider scale[37]. Therefore, it will be important to extend our knowledge on
307 naturally occurring RNA modifications and their impact on innate immune responses. We
308 predict that the analysis of viral RNA modifications will most likely unveil further molecular
309 RNA signatures that function as PAMPs.

310 In summary, our study identifies 2'-*O*-methylation of eukaryotic mRNA cap structures as a
311 molecular pattern of self mRNAs, and demonstrates that there are at least two cellular
312 mechanisms that allow for the distinction of 2'-*O*-methylated versus non-methylated mRNAs.
313 Consequently, a number of viruses replicating in the cytoplasm, without access to the nuclear
314 host cell mRNA capping and modification machinery, have evolved to encode their own RNA-
315 modifying enzymes as means of mimicking cellular mRNAs. Our data should encourage future
316 studies to evaluate the full spectrum and functional significance of mRNA modifications as an
317 additional layer of information imprinted on eukaryotic mRNAs.
318

METHODS SUMMARY

Mice, viruses, cells and virus infection. C57BL/6 mice were obtained from Charles River Laboratories (Sulzfeld, Germany). *ifnar*$^{-/-}$, *mda5*$^{-/-}$, *tlr7*$^{-/-}$, and *mda5*$^{-/-}$ × *tlr7*$^{-/-}$ mice were on the C57BL/6 background and bred in the animal facilities of the Kantonal Hospital St.Gallen. *ifit1*$^{-/-}$ mice were bred in the animal facilities of the Washington University School of Medicine. All mice were maintained in individually ventilated cages and were used between 6 and 9 weeks of age. All animal experiments were done in accordance with the Swiss Federal legislation on animal protection and the Saint Louis University Animal Studies Committees.

HCoV strain 229E, HCoV-D129A, MHV strain A59, MHV-D130A and MHV-Y15A recombinant viruses were generated using a vaccinia virus-based reverse genetic system as described[38] and propagated on either Huh-7 (HCoV) or 17Cl1 (MHV) cells. BHK-21, L929, NIH-3T3, Huh-7, MRC-5 and CV-1 cells were purchased from the European Collection of Cell Cultures. D980R cells were a kind gift from G. L. Smith, Imperial College, London, UK. 17Cl1 cells were a kind gift from S.G. Sawicki, Medical University of Ohio, Toledo, Ohio, USA.

BHK-MHV-N and BHK-HCoV-N cells, expressing the MHV-A59 or HCoV-229E nucleocapsid protein, respectively, under the control of the TET/ON system (Clontech), have been described previously[38]. All cells were maintained in minimal essential medium supplemented with fetal bovine serum (5-10%) and antibiotics. Thioglycolate-elicited murine macrophages were generated as described[39]. Human macrophages were isolated from peripheral blood of normal donors as described[40].

Mice were injected intraperitonealy (i.p.) with 500 p.f.u. of MHV. Organs were stored at –70°C until further analysis. Virus infection of human blood-derived macrophages and thioglycolate-elicited murine macrophages was done in a 24-well format with 0.5-1×10^6 cells and the indicated MOI. MHV titers were determined by standard plaque assay using L929 cells.

343 HCoV titers were determined by plaque assay using Huh-7 cells that were overlaid at 1 h p.i.
344 with 1.2% Avicel/10% DMEM and stained with crystal violet 3 days post infection.

345 **2'-O-methylation of poly(A)-containing RNA *in vitro*.** Poly(A)-containing RNA was
346 isolated using the Dynabeads mRNA DIRECT Kit (Invitrogen, Basel, Switzerland) from 1×10^7
347 mock- or HCoV-infected (MOI=1; at 48 h p.i) Huh-7 cells, and from 1×10^7 mock- or MHV-
348 infected (MOI=1; at 24 h p.i.) NIH-3T3 cells according to the manufacturer's recommendation.
349 The RNA was precipitated after adding 0.1 volume of 4 M ammonium-acetate and 1 volume of
350 isopropanol, washed with 70% ethanol and dissolved in 10 mM TRIS-HCl (pH 7.5) to a final
351 concentration of 150 ng/µl. In vitro 2'-*O*-methylation reactions contained 300 ng of poly(A)-
352 containing RNA derived from virus-infected cells or a corresponding amount of poly(A)-
353 containing RNA from non-infected cells (as determined by qRT-PCR using murine GAPDH and
354 human β-actin specific primers; data not shown) using the ScriptCap 2'-*O*-Methyltransferase
355 (Epicentre Biotechnologies, Madison, USA) in 0.5 µM SAM and 1.4 µM ^{3}H-labeled SAM (78
356 Ci/mmol; Perkin Elmer, Schwerzenbach, Switzerland) for 1 h at 37°C. Reactions were purified
357 using SigmaSpin Post-Reaction Clean-Up columns (Sigma-Aldrich, Buchs, Switzerland), and
358 the eluates were mixed with 2 ml Ultima Gold scintillation fluid to measure ^{3}H-incorporation as
359 counts per minute using a Packard Tri-Carb Liquid Scintillation Counter (Perkin Elmer,
360 Schwerzenbach, Switzerland).

361 **Immunofluorescence, IFN-β ELISA and IFN-α pre-treatment.** Detection of IRF3 was
362 done on thioglycolate-elicited murine macrophages (2×10^5 per well in 200 µl) that were seeded
363 in 8- chamber tissue culture glass slides (BD Falcon), incubated over night at 37°C and infected
364 with MHV at an MOI=1. At 3h p.i. cells were stained for IRF3 (Clone FL-425, Santa Cruz
365 Biotechnology) and DAPI. Images were acquired using a Leica DMRA microscope (Leica,
366 Heerbrugg, Switzerland). Mouse and human IFN-β concentrations in cell culture supernatants

was measured by ELISA (PBL Biomedical Laboratories, NJ, USA) according to manufacturers' instructions. IFN-α pre-treatment of cells prior to virus infection was done using universal type I interferon (IFN-α A/D, Sigma, Buchs, Switzerland).

Bioassay for type I interferon (IFN-I). Total IFN-I in supernatants was measured using LL171 cells (kind gift from M. Pelegrin, Institut de Génétique Moléculaire de Montpellier, France), which are L929 cells stably transfected with a luciferase reporter plasmid under control of the IFN-stimulated response element (ISRE-Luc)[41]. Recombinant IFN-A/D (Sigma) was used as a cytokine standard. Prior to measurement, virus was removed by centrifuging supernatants through AMICON spin columns with a cutoff of 100 kDa (Millipore) according to the manufacturer's instructions. LL171 cells grown in 96-well plates were treated with column-filtered supernatants for 6 hours, and luciferase activity was detected upon addition of Bright-Glo Luciferase substrate (Promega) in a GloMax 96 Plate Luminometer (Promega). All measurements were done in duplicate. The sensitivity threshold of the assay was between 5 and 15 U/ml IFN.

Quantitative RT-PCR. Total cellular RNA was isolated with the NucleoSpin RNA II kit (Macherey-Nagel) according to the manufacturer's instructions and used as template for cDNA synthesis using the High Capacity cDNA Reverse Transcription kit (Applied Biosystems). IFN-β and TATA-box binding protein (TBP) mRNA levels were detected with the LightCycler FastStart DNA Master^{PLUS} SYBR Green I kit (Roche) on a LightCycler 1.5 (Roche). The following primers were used: IFN-β 5'-GGTGGAATGAGACTATTGTTG-3' and 5'-AGGACA TCTCCCACGTC-3', TBP 5'-CCTTCACCAATGACTCCTATGAC-3' and 5'-CAAGTTTACA GCCAAGATTCAC-3'. Measurements were done in duplicate and relative expression of IFN-β was normalized to the mock data by the comparative cycling threshold method ($\Delta\Delta C_T$).

Phylogenetic analysis of viral MTase domains. Regions of MTase homology have been identified previously as members of the RrmJ-like superfamily, InterPro IPR002877. Additional

members of this protein family were identified by BLAST searches using previously-identified RrmJ-like amino acid sequences using the default search parameters. For virus species belonging to a family in which an RrmJ-like domain had been identified, structure-based amino acid alignment was done to determine whether a distant homolog might be present. We compared predicted and actual secondary structures from confirmed 2'-*O*-MTase domains to secondary structure predictions of domains of unknown function. Secondary structures were predicted using PsiPred version 3.0. Putative secondary structure matches were considered as confirmed upon identification of the best-conserved MTase motifs I, IV, VI, VIII and X[42]. Viruses in which we were unable to identify a primary or secondary structure match to RrmJ-like proteins are marked "not detected" in **Supplementary Table 1**.

FIGURE LEGENDS

Figure 1. Conservation of viral 2'-*O*-MTases. **a)** Schematic representation of the human and murine coronavirus genomes. The conserved replicase gene is depicted together with viral proteinase cleavage sites (arrowheads) that separate nsps 1–16. The nsp16-associated 2'-*O*-MTase is depicted. **b)** Coronavirus nsp16 proteins belonging to the human fibrillarin and *E. coli* RrmJ-like methyltransferase family[43] were analyzed by sequence comparison. Sixteen coronavirus nsp16 amino acid sequences, which were 20-90% identical and are representative of alpha-, beta- and gammacoronaviruses were aligned using ClustalW2[44]. Sequence conservation is shown using a color code that indicates the percentage of amino acid identity. Amino acid residues that have been substituted to alanine in previously published biochemical and structural studies[16,18] are colored according to the observed phenotype of the mutant protein. Amino acid-to-alanine replacements characterized in this and previous studies are depicted. **c)** Conservation of viral and cellular methyltransferase motifs. Alignment of MHV nsp16 with homologous

417 methyltransferases from White bream virus (WBV; order *Nidovirales*), Dengue virus (DENV;
418 family *Flaviviridae*), Vesicular stomatitis virus (VSV; order *Mononegavirales*), Vaccinia virus
419 (VACV; family *Poxviridae*), and human fibrillarin (FBL; *Homo sapiens*) was done using
420 ClustalW2 and manually adjusted based on published structural data and PSIPRED protein
421 secondary structure predictions[45]. Motif nomenclature follows Fauman *et al.*[42]. Coloring reflects
422 amino acid similarity and conservation as implemented in JalView[46].
423
424 **Figure 2.** The HCoV 2'-*O*-MTase active site mutant has altered replication kinetics, is
425 defective in ribose 2'-*O*-methylation, induces increased levels of IFN-β, and is IFN-I sensitive. **a)**
426 Analysis of plaques produced by HCoV-229E and HCoV-D129A. **b)** HCoV-229E and HCoV-
427 D129A replication kinetics in MRC-5 cells after infection at an MOI=0.1. Results are the
428 average of two independent experiments done in triplicate. **c)** ^{3}H-incorporation (counts per
429 minute; cpm) into poly(A)-containing RNA derived from mock-infected (self RNA), HCoV-
430 229E-, and HCoV-D129A-infected (non-self RNA) cells after *in vitro* 2'-*O*-methylation using the
431 vaccinia virus 2'-*O*-MTase VP39. Results represent the mean ±SD of three independent
432 experiments. **d)** IFN-β production of human blood-derived MΦs after infection with HCoV-
433 229E and HCoV-D129A. Cells (1×10^{6}) were infected at an MOI=1 and 24 h p.i. IFN-β was
434 measured in the culture supernatant by ELISA. Results are plotted for each of the 9 independent
435 donors and data points from individual donors are connected by lines. Mean values (thick bars)
436 ±SD (thin bars) are indicated and statistical analysis was done using Wilcoxon matched pairs test
437 (**, $p < 0.005$). **e)** Human blood-derived MΦs were pretreated with increasing doses of IFN-α 4
438 h prior to infection with HCoV-229E or HCoV-D129A at MOI=1. At 24 h p.i., supernatants
439 were harvested and viral titers were measured by plaque assay. ND: not detected.
440

Figure 3. MHV 2'-*O*-MTase mutants induce IFN-β in an MDA5-dependent manner. **a)** Poly(A)-containing RNA (300 ng) from MHV-A59, MHV-Y15A and MHV-D130A infected cells was separated on a standard 1% agarose gel and stained with ethidium-bromide (left panel). Genomic and subgenomic mRNAs (mRNA 1-7) and their respective sizes (in kb) are indicated. The right panel shows ^{3}H-incorporation (cpm) into poly(A)-containing RNA derived from mock infected (self RNA), MHV-A59-, MHV-Y15A- and MHV-D130A-infected (non-self RNA) cells after *in vitro* 2'-*O*-methylation using the vaccinia virus 2'-*O*-MTase VP39. Results represent the mean ±SD of seven independent experiments. **b)** Replication kinetics of MHV-A59, MHV-Y15A and MHV-D130A in 17Cl1 cells. Cells were infected at an MOI=1 (left panel) or MOI=0.0001 (right panel), and viral titers in cell culture supernatants were determined at the indicated time points p.i.. **c-e)** Murine MΦs (1×10^{6}) derived from WT (**c**), *ifnar*$^{-/-}$ (**d**), or *mda5*$^{-/-}$ (**e**) mice were infected at an MOI=1 and IFN-β concentration was determined in cell culture supernatants by ELISA at 15 h p.i.. Results represent the mean ±SD of three independent experiments (n=6). **f,g**) Quantitative RT-PCR for IFN-β. WT (**f**), or *ifnar*$^{-/-}$ (**g**) MΦs were infected as described above and IFN-β mRNA expression levels were analyzed by quantitative RT-PCR at the indicated time points. Results represent the mean ±SD of two independent experiments (n=6). Statistical analysis was done using unpaired Student's t-test (***, $p < 0.001$; **, $p < 0.01$; *, $p < 0.05$; n.s. (not significant), $p > 0.05$). ND: not detected.

Figure 4. 2'-*O*-MTase mutant viruses induce nuclear localization of IRF3 in WT, but not MDA5-deficient MΦs. **a)** Detection of IRF3 in MHV-A59, MHV-Y15A or MHV-D130A infected (MOI=1) murine MΦs derived from *ifnar*$^{-/-}$ (upper row) or *mda5*$^{-/-}$ (lower row) mice. Cells were stained at 3 h p.i. for IRF3 (red) and DAPI (blue). Representative fields are shown. **b)** The percentage of cells with IRF3 located in the nucleus was calculated for each

immunofluorescence analysis using five random fields with approximately 50-250 cells each. Results represent the mean ±SD. Statistical analysis was done using unpaired Student's t-test (***, $p < 0.001$; **, $p < 0.01$; *, $p < 0.05$; n.s. (not significant), $p > 0.05$). ND: not detected.

Figure 5. MDA5 is critical for replication restriction of the IFN-I sensitive MHV 2'-*O*-MTase active site mutant MHV-D130A but not for the MHV-Y15A mutant. **a-b)** Murine MΦs (1×10^6) derived from WT (left panels) or MDA5$^{-/-}$ (right panels) mice were infected with MHV-A59, MHV-D130A or MHV-Y15A at an MOI=1 (**a**) or MOI=0.0001 (**b**). Viral titers in the cell culture supernatants were measured at the indicated time points by plaque assay. Results represent the mean ±SEM of two independent experiments (n=5). **c-d)** IFN-sensitivity of MHV 2'-*O*-MTase mutants. Murine MΦs (1×10^5) derived from WT (**c**) or MDA5$^{-/-}$ (**d**) mice were treated with the indicated dosages of IFN-α for 4 h prior to infection (MOI=1) with MHV-A59, MHV-D130A or MHV-Y15A. Viral titers in the cell culture supernatants were measured at 24 h p.i.. Results represent the mean ±SD of two independent experiments (n=4).

Figure 6. MHV replication kinetics in *ifit1*$^{-/-}$ MΦs**. a,b)** Murine MΦs (5×10^5) derived from WT (**a**) or *ifit1*$^{-/-}$ (**b**) mice were infected with MHV-WT, MHV-D130A, or MHV-Y15A at and MOI of 0.01. Viral titers in the cell culture supernatants were measured at the indicated time points by plaque assay. Results represent the mean ±SEM of two independent experiments (n=4).

Figure 7. MHV 2'O-MTase mutants are highly attenuated in WT mice but restore efficient replication in *ifnar*$^{-/-}$ and *mda5*$^{-/-}$/*tlr7*$^{-/-}$ mice. WT, *ifnar*$^{-/-}$, *mda5*$^{-/-}$/*tlr7*$^{-/-}$, *mda5*$^{-/-}$, and *tlr7*$^{-/-}$ mice (6-8 week old) were infected intraperitoneally with 500 p.f.u of MHV-A59, MHV-

D130A or MHV-Y15A. Viral titers in spleens (**a**) and livers (**b**) were determined at 24 h p.i. Results represent the mean ±SD of two independent experiments (n=6). ND: not detected.

ACKNOWLEDGEMENTS

This work was supported by the Swiss National Science Foundation, the Novartis Foundation for Biomedical Research, Switzerland, the German Ministry of Education and Research (to V.T.), the Austrian Science Fund (to M.H.), the Deutsche Forschungsgemeinschaft (to J.Z.), the National Institutes of Health, USA (AI060915 and AI085089 to S.C.B.; U54 AI081680 [Pacific Northwest Regional Center of Excellence for Biodefense and Emerging Infectious Diseases Research] to M.S.D), the Medical Research Council Capacity Building Studentship (to B.W.N.), and the Wellcome Trust (to S.G.S.). The authors are indebted to Lucas Onder for assistance in fluorescence microscopy, and to Rita de Giuli, Barbara Schelle, and Nadja Karl for excellent technical assistance.

AUTHOR CONTRIBUTIONS

R.Z., L.C-B, M.H., R.M., and K.J.S. did most of the experiments. B.W.N. did phylogenetic analyses. B.W.N. and S.C.B. did electron microscopy. J.Z., S.C.B., W.B., M.S.D., S.G.S., and B.L. contributed key research reagents and expertise. S.G.S., B.W.N., B.L., and V.T. conceived and designed the project and wrote and edited the manuscript.

REFERENCES

1. Janeway, C. A., Jr. Approaching the asymptote? Evolution and revolution in immunology. *Cold Spring Harb Symp Quant Biol* **54 Pt 1**, 1-13 (1989).
2. Takeuchi, O. & Akira, S. Innate immunity to virus infection. *Immunol Rev* **227**, 75-86 (2009).
3. Loo, Y. M. & Gale, M., Jr. Viral regulation and evasion of the host response. *Curr Top Microbiol Immunol* **316**, 295-313 (2007).
4. Haller, O. & Weber, F. Pathogenic viruses: smart manipulators of the interferon system. *Curr Top Microbiol Immunol* **316**, 315-34 (2007).
5. Hui, D. J., Terenzi, F., Merrick, W. C. & Sen, G. C. Mouse p56 blocks a distinct function of eukaryotic initiation factor 3 in translation initiation. *J Biol Chem* **280**, 3433-40 (2005).
6. Terenzi, F., Hui, D. J., Merrick, W. C. & Sen, G. C. Distinct induction patterns and functions of two closely related interferon-inducible human genes, ISG54 and ISG56. *J Biol Chem* **281**, 34064-71 (2006).
7. Fensterl, V. & Sen, G. C. The ISG56/IFIT1 Gene Family. *J Interferon Cytokine Res*.
8. Kato, H. et al. Length-dependent recognition of double-stranded ribonucleic acids by retinoic acid-inducible gene-I and melanoma differentiation-associated gene 5. *J Exp Med* **205**, 1601-10 (2008).
9. Hornung, V. et al. 5'-Triphosphate RNA Is the Ligand for RIG-I. *Science* **314**, 994-7 (2006).
10. Pichlmair, A. et al. RIG-I-mediated antiviral responses to single-stranded RNA bearing 5'-phosphates. *Science* **314**, 997-1001 (2006).
11. Schlee, M. et al. Recognition of 5' triphosphate by RIG-I helicase requires short blunt double-stranded RNA as contained in panhandle of negative-strand virus. *Immunity* **31**, 25-34 (2009).
12. Ghosh, A. & Lima, C. D. Enzymology of RNA cap synthesis. *Wiley Interdisciplinary Reviews: RNA* **1**, 152-172 (2010).
13. Shuman, S. What messenger RNA capping tells us about eukaryotic evolution. *Nat Rev Mol Cell Biol* **3**, 619-25 (2002).
14. Nomoto, A., Detjen, B., Pozzatti, R. & Wimmer, E. The location of the polio genome protein in viral RNAs and its implication for RNA synthesis. *Nature* **268**, 208-13 (1977).
15. Hemmi, H. et al. A Toll-like receptor recognizes bacterial DNA. *Nature* **408**, 740-5 (2000).
16. Bouvet, M. et al. In vitro reconstitution of SARS-coronavirus mRNA cap methylation. *PLoS Pathog* **6**, e1000863 (2010).
17. Chen, Y. et al. Functional screen reveals SARS coronavirus nonstructural protein nsp14 as a novel cap N7 methyltransferase. *Proc Natl Acad Sci U S A* **106**, 3484-9 (2009).
18. Decroly, E. et al. Coronavirus nonstructural protein 16 is a cap-0 binding enzyme possessing (nucleoside-2'O)-methyltransferase activity. *J Virol* **82**, 8071-84 (2008).
19. Snijder, E. J. et al. Unique and conserved features of genome and proteome of SARS-coronavirus, an early split-off from the coronavirus group 2 lineage. *J Mol Biol* **331**, 991-1004 (2003).
20. Schnierle, B. S., Gershon, P. D. & Moss, B. Cap-specific mRNA (nucleoside-O2'-)-methyltransferase and poly(A) polymerase stimulatory activities of vaccinia virus are mediated by a single protein. *Proc Natl Acad Sci U S A* **89**, 2897-901 (1992).

21. Cervantes-Barragan, L. et al. Type I IFN-mediated protection of macrophages and dendritic cells secures control of murine coronavirus infection. *J Immunol* **182**, 1099-106 (2009).
22. Cervantes-Barragan, L. et al. Control of coronavirus infection through plasmacytoid dendritic-cell-derived type I interferon. *Blood* **109**, 1131-7 (2007).
23. Rose, K. M., Elliott, R., Martinez-Sobrido, L., Garcia-Sastre, A. & Weiss, S. R. Murine coronavirus delays expression of a subset of interferon-stimulated genes. *J Virol* **84**, 5656-69.
24. Roth-Cross, J. K., Bender, S. J. & Weiss, S. R. Murine coronavirus mouse hepatitis virus is recognized by MDA5 and induces type I interferon in brain macrophages/microglia. *J Virol* **82**, 9829-38 (2008).
25. Zhou, H., Zhao, J. & Perlman, S. Autocrine interferon priming in macrophages but not dendritic cells results in enhanced cytokine and chemokine production after coronavirus infection. *MBio* **1** (2010).
26. Bocharov, G. et al. A Systems Immunology Approach to Plasmacytoid Dendritic Cell Function in Cytopathic Virus Infections. *PLoS Pathog* (in press).
27. Daffis, S. et al. 2′-O methylation of the viral mRNA cap evades host restriction by IFIT family members. *Nature* **468**, 452–456 (2010).
28. Thiel, V. & Weber, F. Interferon and cytokine responses to SARS-coronavirus infection. *Cytokine Growth Factor Rev* **19**, 121-32 (2008).
29. Loo, Y. M. et al. Distinct RIG-I and MDA5 signaling by RNA viruses in innate immunity. *J Virol* **82**, 335-45 (2008).
30. Morin, B. et al. The N-terminal domain of the arenavirus L protein is an RNA endonuclease essential in mRNA transcription. *PLoS Pathog* **6** (2010).
31. Reguera, J., Weber, F. & Cusack, S. Bunyaviridae RNA polymerases (L-protein) have an N-terminal, influenza-like endonuclease domain, essential for viral cap-dependent transcription. *PLoS Pathog* **6** (2010).
32. Qi, X. et al. Cap binding and immune evasion revealed by Lassa nucleoprotein structure. *Nature* (2010).
33. Le Gall, O. et al. Picornavirales, a proposed order of positive-sense single-stranded RNA viruses with a pseudo-T = 3 virion architecture. *Arch Virol* **153**, 715-27 (2008).
34. Gitlin, L. et al. Essential role of mda-5 in type I IFN responses to polyriboinosinic:polyribocytidylic acid and encephalomyocarditis picornavirus. *Proc Natl Acad Sci U S A* **103**, 8459-64 (2006).
35. Nallagatla, S. R. & Bevilacqua, P. C. Nucleoside modifications modulate activation of the protein kinase PKR in an RNA structure-specific manner. *Rna* **14**, 1201-13 (2008).
36. Kariko, K., Buckstein, M., Ni, H. & Weissman, D. Suppression of RNA recognition by Toll-like receptors: the impact of nucleoside modification and the evolutionary origin of RNA. *Immunity* **23**, 165-75 (2005).
37. Nallagatla, S. R., Toroney, R. & Bevilacqua, P. C. A brilliant disguise for self RNA: 5'-end and internal modifications of primary transcripts suppress elements of innate immunity. *RNA Biol* **5**, 140-4 (2008).
38. Eriksson, K. K., Makia, D. & Thiel, V. Generation of recombinant coronaviruses using vaccinia virus as the cloning vector and stable cell lines containing coronaviral replicon RNAs. *Methods Mol Biol* **454**, 237-54 (2008).
39. Zust, R. et al. Coronavirus non-structural protein 1 is a major pathogenicity factor: implications for the rational design of coronavirus vaccines. *PLoS Pathog* **3**, e109 (2007).
40. Wunschmann, S., Becker, B. & Vallbracht, A. Hepatitis A virus suppresses monocyte-to-macrophage maturation in vitro. *J Virol* **76**, 4350-6 (2002).

41. Uze, G. et al. Domains of interaction between alpha interferon and its receptor components. *J Mol Biol* **243**, 245-57 (1994).
42. Fauman, E. B., Blumenthal, R. M. & Chemg, X. in *S-Adenosylmethionine-Dependent Methyltransferases: Structures and Functions* (eds. Cheng, X. & Blumenthal, R. M.) 1-38 (World Scientific, Singapore, 1999).
43. Feder, M., Pas, J., Wyrwicz, L. S. & Bujnicki, J. M. Molecular phylogenetics of the RrmJ/fibrillarin superfamily of ribose 2'-O-methyltransferases. *Gene* **302**, 129-38 (2003).
44. Larkin, M. A. et al. Clustal W and Clustal X version 2.0. *Bioinformatics* **23**, 2947-8 (2007).
45. Bryson, K. et al. Protein structure prediction servers at University College London. *Nucleic Acids Res* **33**, W36-8 (2005).
46. Waterhouse, A. M., Procter, J. B., Martin, D. M., Clamp, M. & Barton, G. J. Jalview Version 2--a multiple sequence alignment editor and analysis workbench. *Bioinformatics* **25**, 1189-91 (2009).

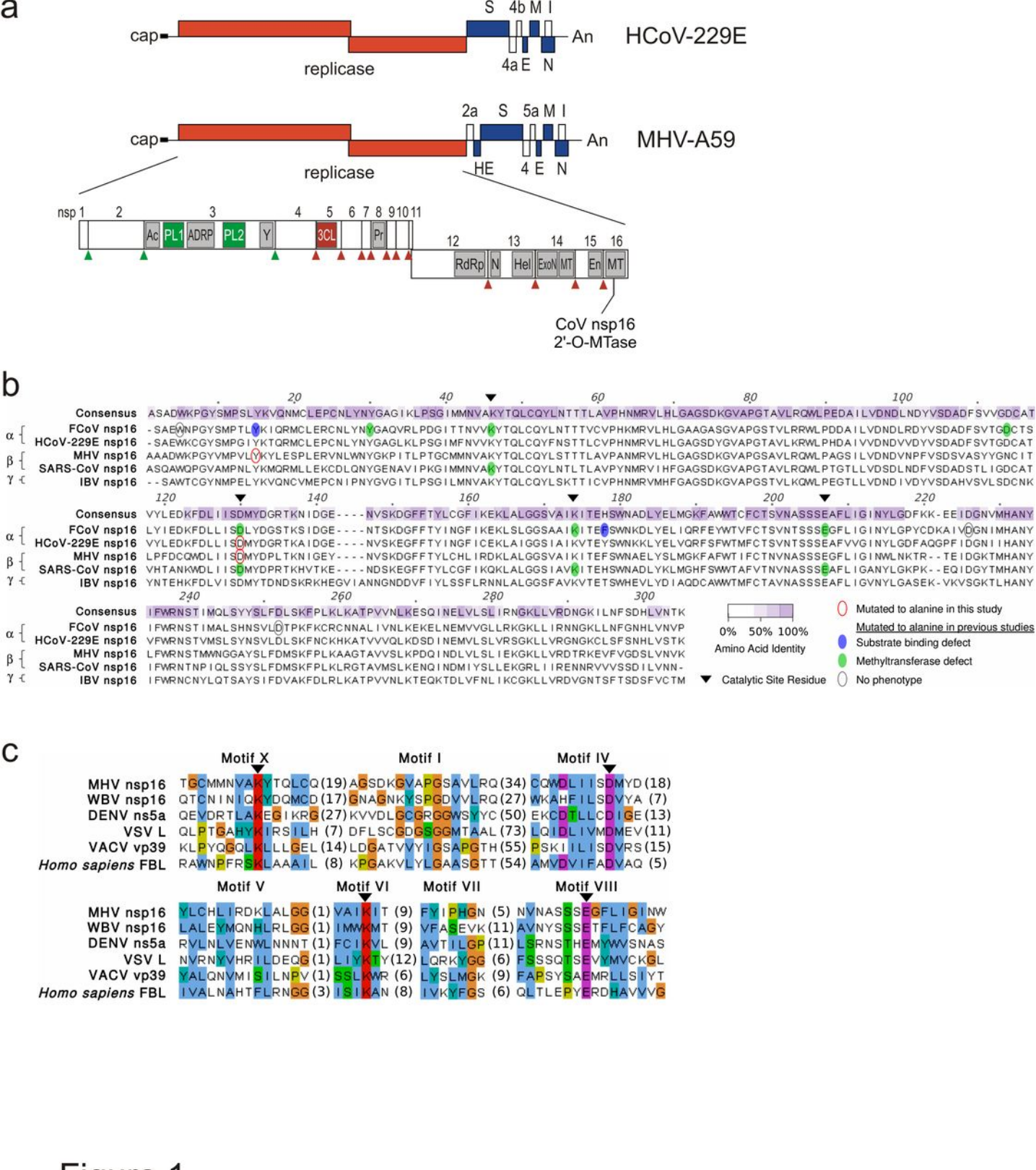
a
cap
replicase
S 4b M I
An
HCoV-229E
4a E N
2a S 5a M I
MHV-A59
HE 4 E N
nsp 1 2 3 4 5 6 7 8 9 10 11
Ac PL1 ADRP PL2 Y 3CL Pr
12 13 14 15 16
RdRp N Hel ExoN MT En MT
CoV nsp16
2'-O-MTase
b
Consensus
FCoV nsp16
HCoV-229E nsp16
MHV nsp16
SARS-CoV nsp16
IBV nsp16
α
β
γ
0% 50% 100%
Amino Acid Identity
Catalytic Site Residue
Mutated to alanine in this study
Mutated to alanine in previous studies
Substrate binding defect
Methyltransferase defect
No phenotype
c
Motif X
Motif I
Motif IV
MHV nsp16
WBV nsp16
DENV ns5a
VSV L
VACV vp39
Homo sapiens FBL
Motif V
Motif VI
Motif VII
Motif VIII

Figure 1

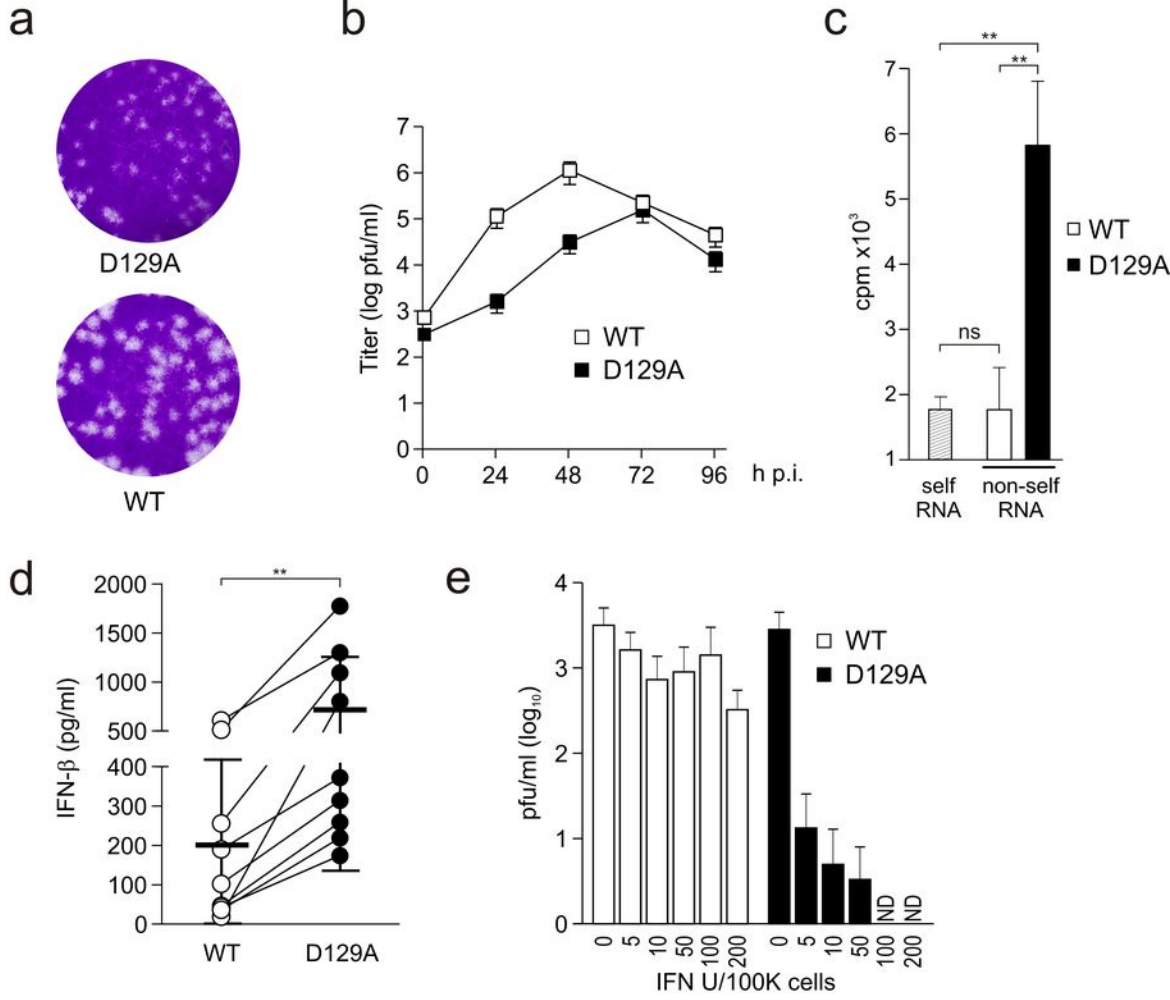
a
D129A
WT
b
Titer (log pfu/ml)
WT
D129A
0
24
48
72
96
h p.i.
c
**
**
cpm x10³
WT
D129A
ns
self RNA
non-self RNA
d
**
IFN-β (pg/ml)
WT
D129A
e
pfu/ml (log₁₀)
WT
D129A
0
5
10
50
100
200
ND
IFN U/100K cells

Figure 2

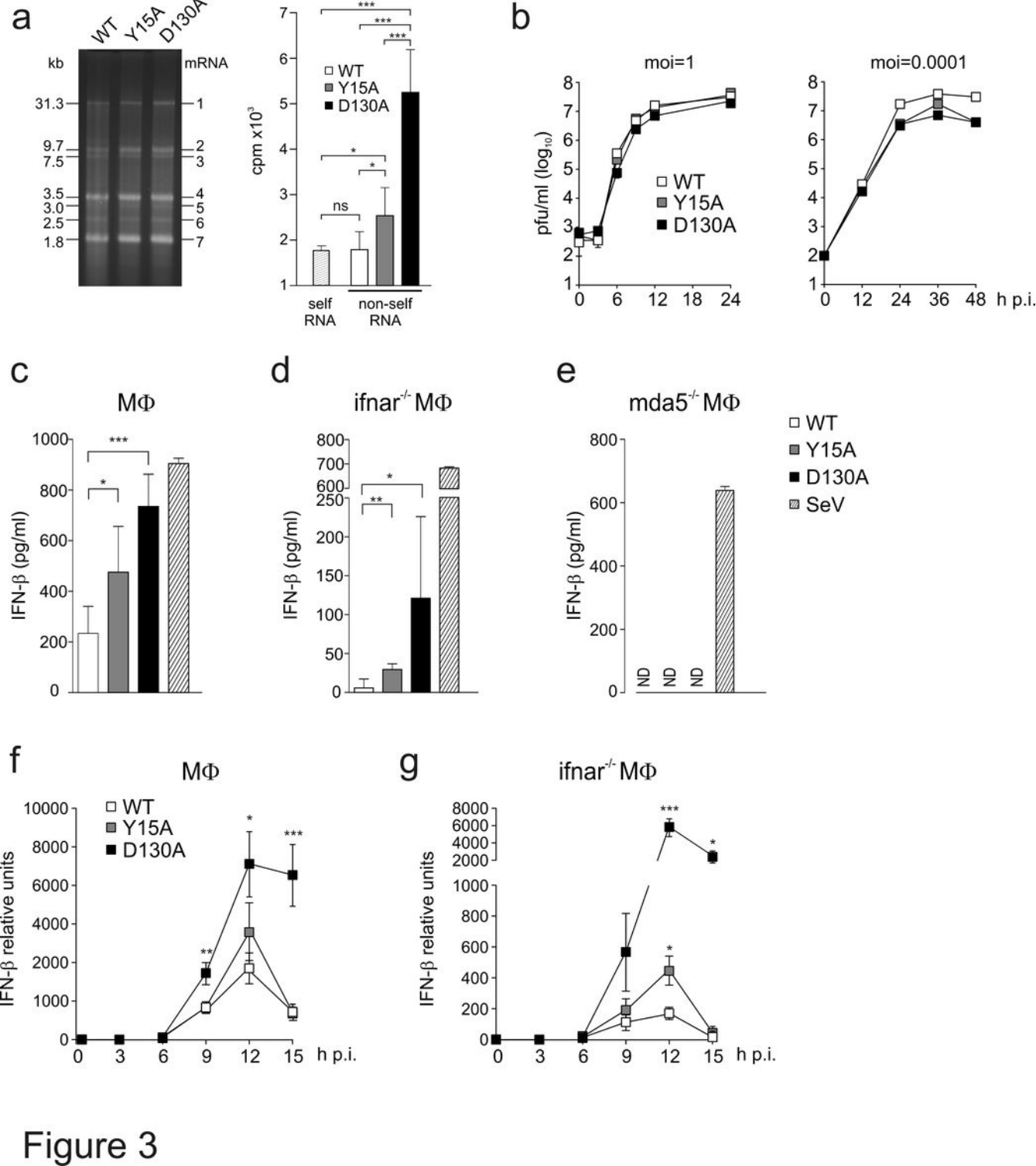
a
WT
Y15A
D130A
kb
mRNA
31.3
9.7
7.5
3.5
3.0
2.5
1.8
1
2
3
4
5
6
7
cpm x10³
WT
Y15A
D130A
ns
self RNA
non-self RNA
b
moi=1
moi=0.0001
pfu/ml (log10)
WT
Y15A
D130A
h p.i.
c
MΦ
IFN-β (pg/ml)
d
ifnar-/- MΦ
IFN-β (pg/ml)
e
mda5-/- MΦ
IFN-β (pg/ml)
ND
WT
Y15A
D130A
SeV
f
MΦ
IFN-β relative units
WT
Y15A
D130A
h p.i.
g
ifnar-/- MΦ
IFN-β relative units
h p.i.

Figure 3

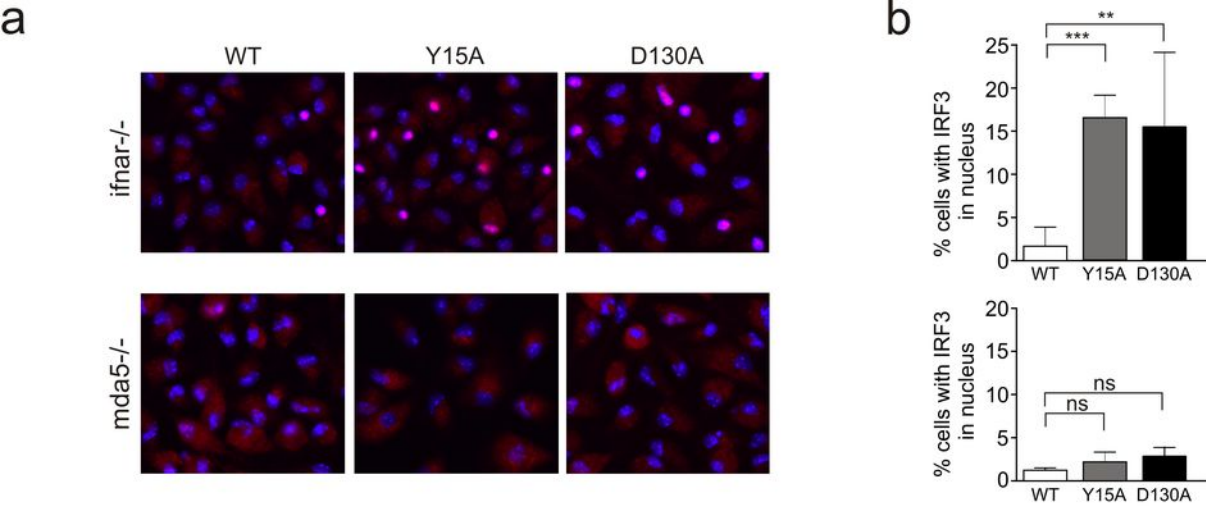
a
WT
Y15A
D130A
ifnar-/-
mda5-/-
b
% cells with IRF3 in nucleus
25
20
15
10
5
0
**
***
WT
Y15A
D130A
% cells with IRF3 in nucleus
20
15
10
5
0
ns
ns
WT
Y15A
D130A

Figure 4

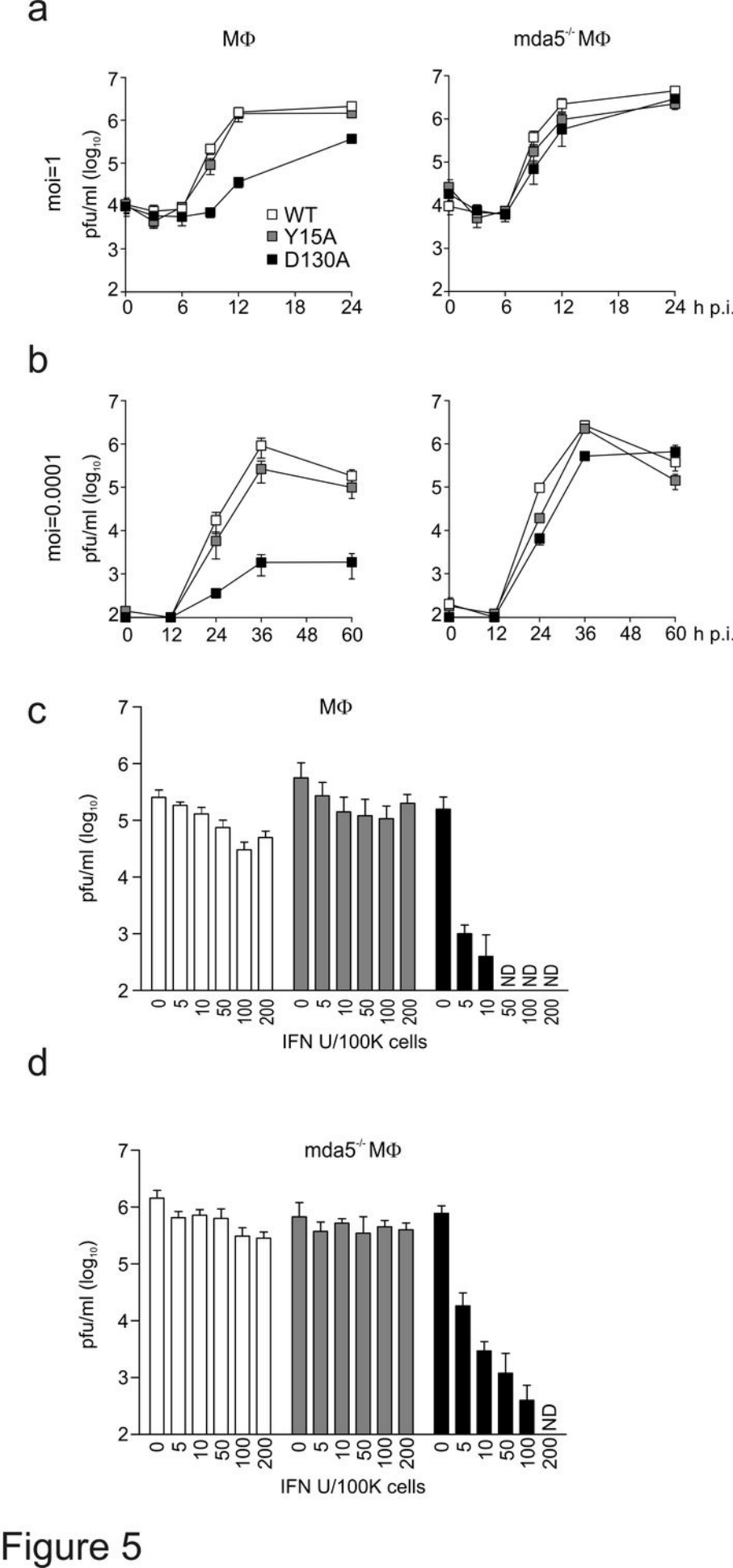
a
MΦ
mda5-/- MΦ
moi=1
pfu/ml (log10)
WT
Y15A
D130A
h p.i.
b
moi=0.0001
c
d
IFN U/100K cells
ND

Figure 5

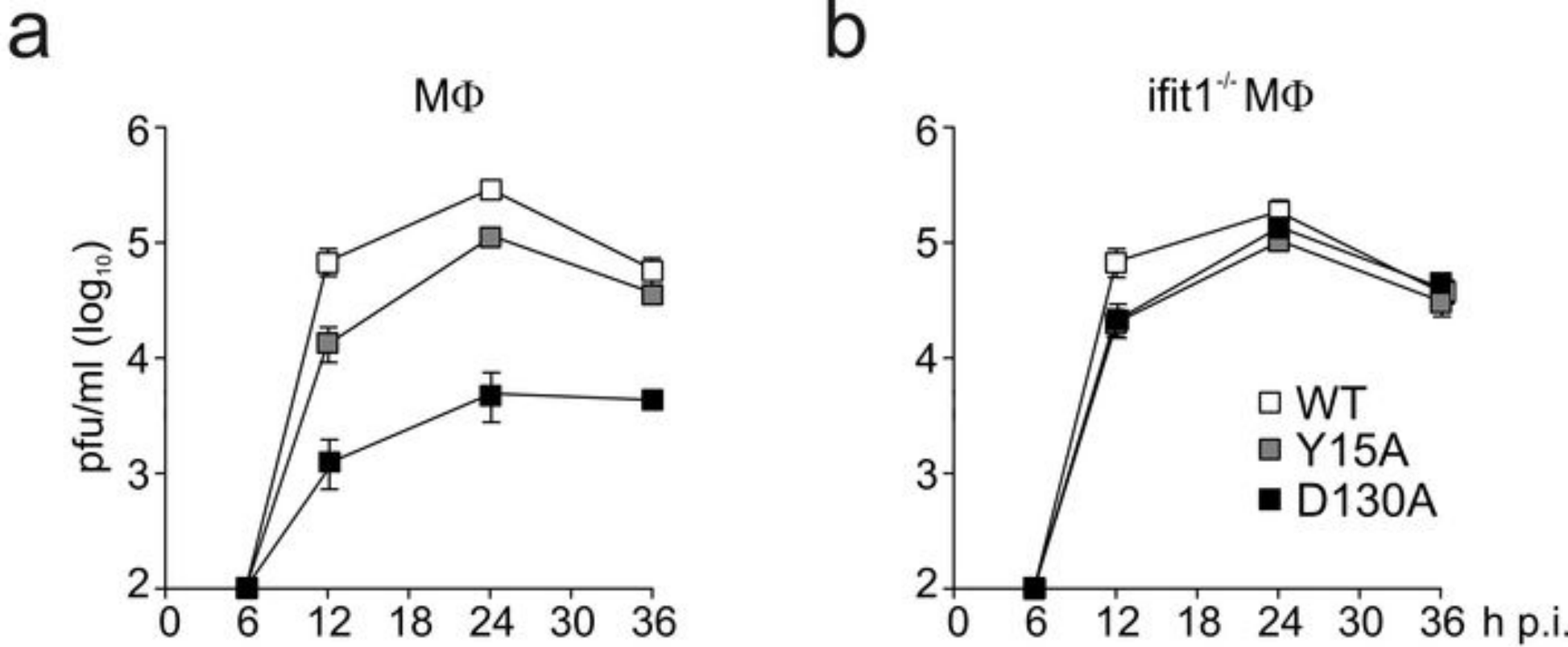
a
MΦ
pfu/ml (log10)
6
5
4
3
2
0
6
12
18
24
30
36
b
ifit1-/- MΦ
WT
Y15A
D130A
h p.i.

Figure 6

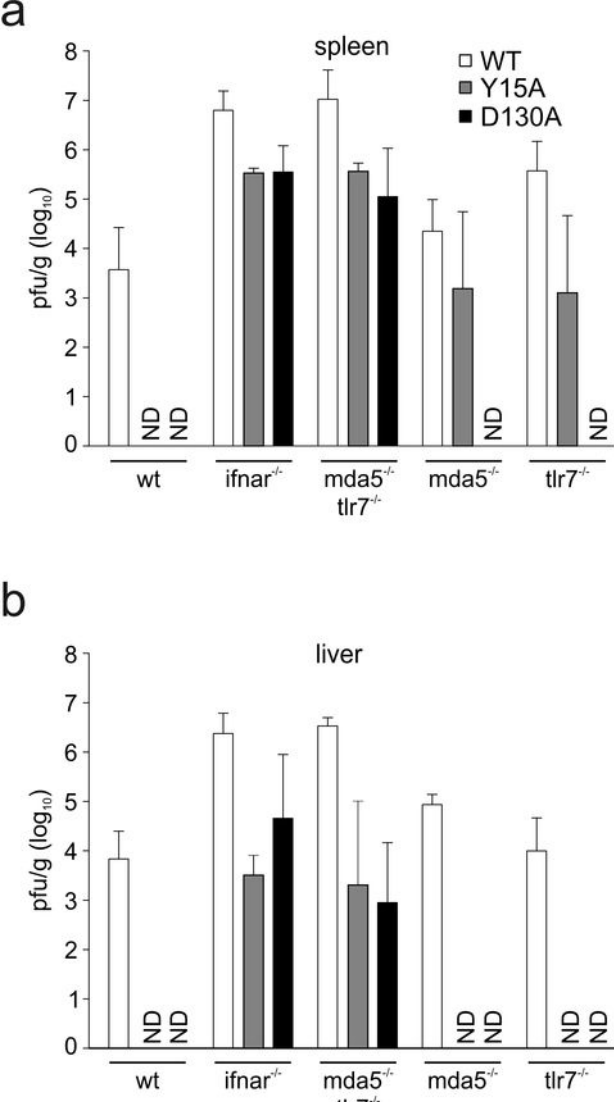
a
spleen
WT
Y15A
D130A
pfu/g (log10)
8
7
6
5
4
3
2
1
0
ND
ND
ND
ND
ND
wt
ifnar-/-
mda5-/- tlr7-/-
mda5-/-
tlr7-/-
b
liver
pfu/g (log10)
8
7
6
5
4
3
2
1
0
ND
ND
ND
ND
ND
wt
ifnar-/-
mda5-/- tlr7-/-
mda5-/-
tlr7-/-

Figure 7